Crystal Structure, Charge-Transfer-Induced Spin Transition, and Photoreversible Magnetism in a Cyano-Bridged Cobalt−Tungstate Bimetallic Assembly

Shin-ichi Ohkoshi,*[,†] Yoshiho Hamada,[†] Tomoyuki Matsuda,[†] Yoshihide Tsunobuchi,[†] and Hiroko Tokoro[†,‡]

Department of Chemistry, School of Science, The University of Tokyo, 7-3-1 Hongo, Bunkyo-ku, Tokyo 113-0033 Japan, and PRESTO, JST, 4-1-8 Honcho Kawaguchi, Saitama 332-0012, Japan

Received November 15, 2007. Revised Manuscript Received December 27, 2007

This paper describes the crystal structure, magnetic properties, and photoreversible magnetic properties of $Co^{II}_3[W^V(CN)_8]_2(pyrimidine)_4 \cdot 6H_2O$. We found that complexes of this formula had two types of crystal structures ($[\{Co^{II}(pyrimidine)_2\}_2\{Co^{II}(H_2O)_2\}\{W^V(CN)_8\}_2] \cdot 4H_2O$ (**1**) and $[\{Co^{II}(pyrimidine)(H_2O)\}_2\{Co^{II}(H_2O)_2\}\{W^V(CN)_8\}_2](pyrimidine)_2 \cdot 2H_2O$ (**2**)). These two structures had similar metal−organic frameworks but differed in the coordination environment around Co1, i.e., $Co1(NC)_4(pyrimidine)_2$ in **1** and $Co1(NC)_4(pyrimidine)(H_2O)$ in **2**. In **1**, a temperature-induced phase transition from the Co^{II} ($S = 3/2$)−NC−W^V ($S = 1/2$) [high-temperature (HT)] phase to the Co^{III} ($S = 0$)−NC−W^{IV} ($S = 0$) [low-temperature (LT)] phase was observed due to a charge-transfer-induced spin transition. However, **2** did not exhibit such a phase transition. When the LT phase of **1** was irradiated by 840 nm light, ferromagnetism with a Curie temperature of 40 K and magnetic coercive field of 12 kOe were observed. UV–vis reflectance and infrared measurements suggested that the LT phase optically transited to the photoinduced (PI) phase, which had a similar valence state as the HT phase, through the metal-to-metal charge-transfer ($W^{IV} \rightarrow Co^{III}$) band. In contrast, when the back metal-to-metal charge transfer ($Co^{II} \rightarrow W^V$) band of the PI phase was excited by 532 nm light, the reverse phase transition from the PI phase to the LT phase occurred, and the spontaneous magnetization decreased.

1. Introduction

In the field of molecule-based magnets, cyano-bridged metal assemblies are aggressively studied to demonstrate novel functionalities.[1] Hexacyanometalate-based materials show interesting functionalities such as high Curie temperatures,[2] temperature-induced phase transitions,[3] and external stimuli-induced magnetism.[4–10] Recently, octacyanometalate-based magnets have drawn much attention.[11–20] Octacyanometalates $[M(CN)_8]^{n-}$ (M = Mo, W, etc.) are a versatile class of building blocks, which can adopt different spatial configurations that depend on the chemical environment, e.g., square antiprism (D_{4h}), dodecahedron (D_{2d}), and bicapped trigonal prism (C_{2v}). Metal assemblies based on $[M(CN)_8]^{n-}$ can take various coordination geometries in the crystal structure, that is, zero-dimensional (0-D),[12] 1-D,[13,14] 2-D,[15–18] and 3-D structures.[19,20] For example, 0-D structural clusters of $\{Mn_9^{II}[W^V(CN)_8]_6 \cdot 24C_2H_5OH\} \cdot 12C_2H_5OH$[12a] and $\{Mn_9^{II}[Mo^V(CN)_8]_6 \cdot 24CH_3OH\} \cdot 5CH_3OH \cdot 2H_2O$,[12b] 1-D linear

* Corresponding author: e-mail ohkoshi@chem.s.u-tokyo.ac.jp; Tel +81-3-5841-4331; Fax +81-3-3812-1896.

† The University of Tokyo.

‡ PRESTO.

(1) (a) Verdaguer, M.; Bleuzen, A.; Train, C.; Garde, R.; Fabrizi de Biani, F.; Desplanches, C. *Philos. Trans. R. Soc. London, Ser. A* **1999**, *357*, 2959. (b) Miller, J. S. *Mater. Res. Soc. Bull.* **2000**, *25*, 60. (c) Ohkoshi, S.; Hashimoto, K. *J. Photochem. Photobiol. C* **2001**, *2*, 71. (d) Dunbar, K. R.; Heintz, R. A. *Prog. Inorg. Chem.* **1997**, *45*, 283.

(2) (a) Ferlay, S.; Mallah, T.; Ouahès, R.; Veillet, P.; Verdaguer, M. *Nature (London)* **1995**, *378*, 701. (b) Holmes, S. M.; Girolami, G. S. *J. Am. Chem. Soc.* **1999**, *121*, 5593. (c) Hatlevik, Ø.; Buschmann, W. E.; Zhang, J.; Manson, J. L.; Miller, J. S. *Adv. Mater.* **1999**, *11*, 914. (d) Ohkoshi, S.; Mizuno, M.; Hung, G. J.; Hashimoto, K. *J. Phys. Chem. B* **2000**, *104*, 9365.

(3) (a) Shimamoto, N.; Ohkoshi, S.; Sato, O.; Hashimoto, K. *Inorg. Chem.* **2002**, *41*, 678. (b) Tokoro, H.; Ohkoshi, S.; Matsuda, T.; Hashimoto, K. *Inorg. Chem.* **2004**, *43*, 5231. (c) Bleuzen, A.; Escax, V.; Ferrier, A.; Villain, F.; Verdaguer, M.; Münsch, P.; Itié, J.-P. *Angew. Chem., Int. Ed.* **2004**, *43*, 3728. (d) Kosaka, W.; Nomura, K.; Hashimoto, K.; Ohkoshi, S. *J. Am. Chem. Soc.* **2005**, *127*, 8590. (e) Tokoro, H.; Miyashita, S.; Hashimoto, K.; Ohkoshi, S. *Phys. Rev. B* **2006**, *73*, 172415.

(4) (a) Dei, A. *Angew. Chem., Int. Ed.* **2005**, *44*, 1160. (b) Sato, O.; Iyoda, T.; Fujishima, A.; Hashimoto, K. *Science* **1996**, *272*, 704. (c) Ohkoshi, S.; Yorozu, S.; Sato, O.; Iyoda, T.; Fujishima, A.; Hashimoto, K. *Appl. Phys. Lett.* **1997**, *70*, 1040. (d) Bleuzen, A.; Lomenech, C.; Escax, V.; Villain, F.; Varret, F.; Cartier dit Moulin, C.; Verdaguer, M. *J. Am. Chem. Soc.* **2000**, *122*, 6648. (e) Pejakovic, D. A.; Manson, J. L.; Miller, J. S.; Epstein, A. J. *Phys. Rev. Lett.* **2000**, *85*, 1994. (f) Tokoro, H.; Ohkoshi, S.; Hashimoto, K. *Appl. Phys. Lett.* **2003**, *82*, 1245.

(5) (a) Margadonna, S.; Prassides, K.; Fitch, A. N. *Angew. Chem., Int. Ed.* **2004**, *43*, 6316. (b) Papanikolaou, D.; Margadonna, S.; Kosaka, W.; Ohkoshi, S.; Brunelli, M.; Prassides, K. *J. Am. Chem. Soc.* **2006**, *128*, 8358.

(6) (a) Coronado, E.; Giménez-López, M. C.; Levchenko, G.; Romero, F. M.; García-Baonza, V.; Milner, A.; Paz-Pasternak, M. *J. Am. Chem. Soc.* **2005**, *127*, 4580. (b) Egan, L.; Kamenev, K.; Papanikolaou, D.; Takabayashi, Y.; Margadonna, S. *J. Am. Chem. Soc.* **2006**, *128*, 6034.

(7) (a) Ohkoshi, S.; Arai, K.; Sato, Y.; Hashimoto, K. *Nat. Mater.* **2004**, *3*, 857. (b) Yanai, N.; Kaneko, W.; Yoneda, K.; Ohba, M.; Kitagawa, S. *J. Am. Chem. Soc.* **2007**, *129*, 3496.

(8) (a) Margadonna, S.; Prassides, K.; Fitch, A. N. *J. Am. Chem. Soc.* **2004**, *126*, 15390. (b) Goodwin, A. L.; Chapman, K. W.; Kepert, C. J. *J. Am. Chem. Soc.* **2005**, *127*, 17980. (c) Chapman, K. W.; Chupas, P. J.; Kepert, C. J. *J. Am. Chem. Soc.* **2006**, *128*, 7009.

(9) Ohkoshi, S.; Tokoro, H.; Matsuda, T.; Takahashi, H.; Irie, H.; Hashimoto, K. *Angew. Chem., Int. Ed.* **2007**, *46*, 3238.

(10) Kaye, S. S.; Long, J. R. *J. Am. Chem. Soc.* **2005**, *127*, 6506.

(11) (a) Sieklucka, B.; Podgajny, R.; Korzeniak, T.; Przychodzeń, P.; Kania, R. *C. R. Chim.* **2002**, *5*, 639. (b) Przychodzeń, P.; Korzeniak, T.; Podgajny, R.; Sieklucka, B. *Coord. Chem. Rev.* **2006**, *250*, 2234.

10.1021/cm703258n CCC: $40.75
Published on Web 02/05/2008

chain compounds of $[Cu^{II}(tetraethylenepentaamineH_2)]_2[W^{IV}(CN)_8]_2\cdot 5H_2O$,[13b] and $Sm^{III}(terpyridine)(dimethylformamide)_4[W^{V}(CN)_8]\cdot 8H_2O$,[14c] 2-D grid layer compounds of $[Cu^{II}(tetraazacyclodecane)]_2[Mo^{IV}(CN)_8]\cdot 10.5H_2O$,[15a] $(tetraethylenepentaamineH_5)_{0.8}Cu^{II}_4[W^{V}(CN)_8]_4\cdot 7.2H_2O$,[16a] and $Cs[\{Co^{II}(3\text{-cyanopyridine})_2\}\{W^{V}(CN)_8\}]\cdot H_2O$,[18] and 3-D structural compounds of $Mn^{II}_6(H_2O)_9\{W^{V}(CN)_8\}_4\cdot 13H_2O$,[19b] $\{W^{V}(CN)_2\}_2\{(\mu\text{-}CN)_4Co^{II}(H_2O)_2\}_3\cdot 4H_2O$,[19d] and $Cu^{II}_3[W^{V}(CN)_8]_2(pyrimidine)_2\cdot 8H_2O$[19h] have been reported. One attractive issue in the field of molecule-based magnets is to develop magneto-optical functionalities, such as a Faraday effect,[21] a nonlinear magnetooptical effect,[22] and a photomagnetic effect.[4,18,20,23] One possible method to achieve the photomagnetic effect, i.e., optical control of the spontaneous magnetization, is to change the electronic spin state of a magnetic material. For example, when irradiating changes the oxidation numbers of the transition metal ions in a magnetic material, its magnetization is varied. Structural flexibility is also important to maintain the valence isomer. From these viewpoints, octacyanometalate-based compounds are useful systems for preparing photomagnetic materials because octacyanometalates can adopt various valence states, e.g., $Mo^{IV/V}$ and $W^{IV/V}$, and octacyanometalates can adopt various spatial configurations.[24] As an example of this scenario, we have recently observed the photoinduced magnetization on a cyano-bridged cobalt−tungstate bimetallic assembly, $Co^{II}_3[W^{V}(CN)_8]_2(pyrimidine)_4\cdot 6H_2O$, and reported the preliminary results of this phenomenon.[20c] In the present work, we found that a $Co^{II}_3[W^{V}(CN)_8]_2(pyrimidine)_4\cdot 6H_2O$ solid has two similar crystal structures ($[\{Co^{II}(pyrimidine)_2\}_2\{Co^{II}(H_2O)_2\}\{W^{V}(CN)_8\}_2]\cdot 4H_2O$ (**1**) and $[\{Co^{II}(pyrimidine)(H_2O)\}_2\{Co^{II}(H_2O)_2\}\{W^{V}(CN)_8\}_2](pyrimidine)_2\cdot 2H_2O$ (**2**)). Compound **1** exhibits a charge-transfer-induced spin transition and a photoreversible magnetic effect upon irradiation with two different wavelengths of light, although **2** does not exhibit such phenomena. Herein, we complete the study by reporting (i) the crystal structure, (ii) magnetic properties, (iii) charge-transfer-induced phase transition, (iv) photoreversible magnetization, and (v) the mechanism of the photoreversible magnetism.

2. Experimental Section

2.1. Synthesis. The powder-form compound **1** was prepared by adding 2.5 mL of $Cs^{I}_3[W^{V}(CN)_8]\cdot 2H_2O$[25] (0.12 mol dm^{-3}) aqueous solution to 2.5 mL of a mixed aqueous solution of $Co^{II}Cl_2\cdot 6H_2O$ (0.19 mol dm^{-3}) and pyrimidine (0.25 mol dm^{-3}). The precipitated powder was filtered, washed with water, and then dried in air. Inductively coupled plasma mass spectrometry and standard microanalytical methods confirmed that the formula of **1** was $Co^{II}_3[W^{V}(CN)_8]_2(pyrimidine)_4\cdot 6H_2O$: Calculated: Co, 12.73; W, 26.46; C, 27.67; H, 2.03; N, 24.20%. Found: Co, 12.55; W, 26.44; C, 27.75; H, 1.92; N, 24.48%. In the infrared (IR) spectra, CN stretching peaks were observed at 2185, 2171, and 2160 cm^{-1}. Furthermore, when **1** was kept in solution for a long time, **2** appeared (Scheme 1). **2** was filtered, washed with water, and then dried in air. The formula of **2** was $Co^{II}_3[W^{V}(CN)_8]_2(pyrimidine)_4\cdot 6H_2O$, which was identical to that of **1**: Calculated: Co, 12.73; W, 26.46; C, 27.67; H, 2.03; N, 24.20%. Found: Co, 12.59; W, 26.48; C, 27.47; H, 2.03; N, 24.09%. In the IR spectra, CN stretching peaks were observed at 2186, 2180, 2176, 2172,

(12) (a) Zhong, Z. J.; Seino, H.; Mizobe, Y.; Hidai, M.; Fujishima, A.; Ohkoshi, S.; Hashimoto, K. *J. Am. Chem. Soc.* **2000**, *122*, 2952. (b) Larionova, J.; Gross, M.; Pilkington, M.; Andres, H.; Stoeckli-Evans, H.; Güdel, H. U.; Decurtins, S. *Angew. Chem., Int. Ed.* **2000**, *39*, 1605. (c) Sieklucka, B.; Szklarzewicz, J. *Inorg. Chem.* **2000**, *39*, 5156. (d) Bonadio, F.; Gross, M.; Stoeckli-Evans, H.; Decurtins, S. *Inorg. Chem.* **2002**, *41*, 5891. (e) Herrera, J. M.; Marvaud, V.; Verdaguer, M.; Marrot, J.; Kalisz, M.; Mathonière, C. *Angew. Chem., Int. Ed.* **2004**, *43*, 2. (f) Song, Y.; Zhang, P.; Ren, X.-M.; Shen, X.-F.; Li, Y.-Z.; You, X.-Z. *J. Am. Chem. Soc.* **2005**, *127*, 3708. (g) Freedman, D. E.; Bennett, M. V.; Long, J. R. *Dalton Trans.* **2006**, *23*, 2829. (h) Lim, J. H.; Yoon, J. H.; Kim, H. C.; Hong, C. S. *Angew. Chem., Int. Ed.* **2006**, *45*, 7424.

(13) (a) Rombaut, G.; Golhen, S.; Ouahab, L.; Mathonière, C.; Kahn, O. *J. Chem. Soc., Dalton Trans.* **2000**, 3609. (b) Podgajny, R.; Korzeniak, T.; Stadnicka, K.; Dromzée, Y.; Alcock, N. W.; Errington, W.; Kruczała, K.; Balanda, M.; Kemp, T. J.; Verdaguer, M.; Sieklucka, B. *Dalton Trans.* **2003**, 3458. (c) Pradhan, R.; Desplanches, C.; Guionneau, P.; Sutter, J.-P. *Inorg. Chem.* **2003**, *42*, 6607. (d) Li, D.; Zheng, L.; Zhang, Y.; Huang, J.; Gao, S.; Tang, W. *Inorg. Chem.* **2003**, *42*, 6123. (e) You, Y. S.; Kim, D.; Do, Y.; Oh, S. J.; Hong, C. S. *Inorg. Chem.* **2004**, *43*, 6899.

(14) (a) Ikeda, S.; Hozumi, T.; Hashimoto, K.; Ohkoshi, S. *Dalton Trans.* **2005**, 2120. (b) Matoga, D.; Mikuriya, M.; Handa, M.; Szklarzewicz, J. *Chem. Lett.* **2005**, *34*, 1550. (c) Przychodzeń, P.; Lewiński, K.; Pelka, R.; Balanda, M.; Tomala, K.; Sieklucka, B. *Dalton Trans.* **2006**, 625. (d) Prins, F.; Pasca, E.; Jongh, L. J.; Kooijman, H.; Spek, A. L.; Tanase, S. *Angew. Chem., Int. Ed.* **2007**, *46*, 6081.

(15) (a) Larionova, J.; Clérac, R.; Donnadieu, B.; Willemin, S.; Guérin, C. *Cryst. Growth Des.* **2003**, *3*, 267. (b) Korzeniak, T.; Stadnicka, K.; Rams, M.; Sieklucka, B. *Inorg. Chem.* **2004**, *43*, 4811.

(16) (a) Podgajny, R.; Korzeniak, T.; Balanda, M.; Wasiutynski, T.; Errington, W.; Kemp, T. J.; Alcock, N. W.; Sieklucka, B. *Chem. Commun.* **2002**, 1138. (b) Hozumi, T.; Ohkoshi, S.; Arimoto, Y.; Seino, H.; Mizobe, Y.; Hashimoto, K. *J. Phys. Chem. B* **2003**, *107*, 11571. (c) Kaneko, S.; Tsunobuchi, Y.; Sakurai, S.; Ohkoshi, S. *Chem. Phys. Lett.* **2007**, *446*, 292.

(17) Ohkoshi, S.; Arimoto, Y.; Hozumi, T.; Seino, H.; Mizobe, Y.; Hashimoto, K. *Chem. Commun.* **2003**, 2772.

(18) Arimoto, Y.; Ohkoshi, S.; Zhong, Z. J.; Seino, H.; Mizobe, Y.; Hashimoto, K. *J. Am. Chem. Soc.* **2003**, *125*, 9240.

(19) (a) Garde, R.; Desplanches, C.; Bleuzen, A.; Veillet, P.; Verdaguer, M. *Mol. Cryst. Liq. Cryst.* **1999**, *334*, 587. (b) Zhong, Z. J.; Seino, H.; Mizobe, Y.; Hidai, M.; Verdaguer, M.; Ohkoshi, S.; Hashimoto, K. *Inorg. Chem.* **2000**, *39*, 5095. (c) Song, Y.; Ohkoshi, S.; Arimoto, Y.; Seino, H.; Mizobe, Y.; Hashimoto, K. *Inorg. Chem.* **2003**, *42*, 1848. (d) Herrera, J. M.; Bleuzen, A.; Dromzée, Y.; Julve, M.; Lloret, F.; Verdaguer, M. *Inorg. Chem.* **2003**, *42*, 7052. (e) Kashiwagi, T.; Ohkoshi, S.; Seino, H.; Mizobe, Y.; Hashimoto, K. *J. Am. Chem. Soc.* **2004**, *126*, 5024. (f) Withers, J. R.; Li, D.; Triplet, J.; Ruschman, C.; Parkin, S.; Wang, G.; Yee, G. T.; Holmes, S. M. *Inorg. Chem.* **2006**, *45*, 4307. (g) Wang, Z.-X.; Shen, X.-F.; Wang, J.; Zhang, P.; Li, Y.-Z.; Nfor, E. N.; Song, Y.; Ohkoshi, S.; Hashimoto, K.; You, X.-Z. *Angew. Chem., Int. Ed.* **2006**, *45*, 3287. (h) Ohkoshi, S.; Tsunobuchi, Y.; Takahashi, H.; Hozumi, T.; Shiro, M.; Hashimoto, K. *J. Am. Chem. Soc.* **2007**, *129*, 3084.

(20) (a) Hozumi, T.; Hashimoto, K.; Ohkoshi, S. *J. Am. Chem. Soc.* **2005**, *127*, 3864. (b) Ohkoshi, S.; Tokoro, H.; Hozumi, T.; Zhang, Y.; Hashimoto, K.; Mathonière, C.; Bord, I.; Rombaut, G.; Verelst, M.; Cartier dit Moulin, C.; Villain, F. *J. Am. Chem. Soc.* **2006**, *128*, 270. (c) Ohkoshi, S.; Ikeda, S.; Hozumi, T.; Kashiwagi, T.; Hashimoto, K. *J. Am. Chem. Soc.* **2006**, *128*, 5320.

(21) Ohkoshi, S.; Mizuno, M.; Hung, G. J.; Hashimoto, K. *J. Phys. Chem. B* **2000**, *104*, 9365.

(22) (a) Aktsipetrov, O. A.; Braginskii, O. V.; Esikov, D. A. *Sov. J. Quantum Electron.* **1990**, *20*, 259. (b) Ikeda, K.; Ohkoshi, S.; Hashimoto, K. *Chem. Phys. Lett.* **2001**, *349*, 371. (c) Ikeda, K.; Ohkoshi, S.; Hashimoto, K. J. *Appl. Phys* **2003**, *93*, 1371. (d) Nuida, T.; Matsuda, T.; Tokoro, H.; Sakurai, S.; Hashimoto, K.; Ohkoshi, S. *J. Am. Chem. Soc.* **2005**, *127*, 11604.

(23) Takahashi, Y.; Suemoto, T.; Oguri, S.; Takeda, J. *Phys. Rev. B* **2006**, *74*, 193104.

(24) (a) Hennig, H.; Rehorek, A.; Rehorek, D.; Thomas, P. *Inorg. Chim. Acta* **1984**, *86*, 41. (b) Rehorek, D.; Salvetter, J.; Hantschmann, A.; Hennig, H.; Stasicka, Z.; Chodkowska, A. *Inorg. Chim. Acta* **1979**, *37*, L471. (c) Hennig, H.; Rehorek, A.; Rehorek, D.; Thomas, P. *Inorg. Chim. Acta* **1983**, *77*, L11.

(25) Bok, L. D. C.; Leipoldt, J. G.; Basson, S. S. *Z. Anorg. Allg. Chem.* **1975**, *415*, 81.

Scheme 1

$$3Co^{2+} + 2[W(CN)_8]^{3-} + 4\text{pyrimidine} \xrightarrow[H_2O]{} \text{Compound } \mathbf{1} \xrightarrow[H_2O]{} \text{Compound } \mathbf{2}$$

2167, 2162, and 2154 cm^{-1}. As for **2**, a single crystal was prepared by a diffusion method in an H-shaped tube.

2.2. Physical Characterization. The morphologies of the compounds were measured by a Hitachi S 4200 scanning electron microscope (SEM) with a 10 kV accelerating voltage. The X-ray powder diffraction (XRD) patterns were measured by a Rigaku RINT2100 with Cu Kα radiation ($\lambda = 1.5406$ Å) at 293 K. Rietveld analyses were performed by the RIETAN-FP program.[26] Single-crystal X-ray data were collected on a Rigaku R-AXIS RAPID imaging plate area detector with graphite monochromated Mo Kα radiation. The IR spectra were recorded on a Shimadzu FT-IR 8200PC spectrometer. The UV–vis reflectance spectra were measured by a Shimazu UV-3100 spectrometer. The magnetic susceptibility and magnetization measurements were conducted using a Quantum Design MPMS superconducting quantum interference device (SQUID) magnetometer.

2.3. Light Irradiation Experiment. A light irradiation experiment inside the SQUID was carried out using continuous wave (CW) diode lasers with $\lambda = 840$ and 532 nm as the light sources. The powder-form sample spread on adhesive tape was placed on the edge of an optical fiber in the SQUID. Light irradiation measurements in IR spectroscopy were carried out using 840 and 532 nm diode laser lights. The powder-form sample was spread on CaF_2 plate, and the sample temperature was controlled by an Oxford Instruments cryostat.

3. Results and Discussion

3.1. Crystal Structure. *Compound 1.* SEM image showed that **1** was composed of plate-type microcrystals with an average size of 0.9 × 0.7 × 0.1 μm (Figure S1a). Figure 1a shows the XRD pattern of **1** in the powder form. Rietveld analysis indicated that the sample has a monoclinic crystal structure in the $P2_1/n$ space group ($a = 7.5758(12)$ Å, $b = 13.875(2)$ Å, $c = 22.230(4)$ Å, $\beta = 95.709(7)°$, and $Z = 2$) with refinements of $R_{wp} = 9.96\%$ and $R_p = 6.94\%$ (Tables 1 and S1). It is noted that this analysis was based on the analogous crystal structure of $[\{Co^{II}/Cu^{II}(\text{pyrimidine})_2\}_2\{Co^{II}/Cu^{II}(H_2O)_2\}\{W^{V}(CN)_8\}_2]\cdot 4H_2O$ (Co^{II}:Cu^{II} = 2:1), which was obtained by mixing metal cations of Co^{II} and Cu^{II} in the synthetic procedure (Figure S2 and Table S2). The asymmetric unit consisted of a $[W(CN)_8]^{3-}$ anion, a $[Co1(\text{pyrimidine})_2]^{2+}$ cation, one-half of a $[Co2(H_2O)_2]^{2+}$ cation, and two zeolitic waters (Figure 1b). The coordination geometries of the Co (Co1 and Co2) and W sites were pseudo-octahedron (D_{4h}) and bicapped trigonal prism (C_{2v}), respectively. The four equatorial positions of Co1 were occupied by cyanide nitrogen atoms of $[W(CN)_8]$, while the apical positions were occupied by two nitrogen atoms of the pyrimidine. Co2 was coordinated to two nitrogen atoms of $[W(CN)_8]$, two oxygen atoms of the water ligands, and two nitrogen atoms of the pyrimidines. The five CN groups of $[W(CN)_8]$ were bridged to four Co1 and one Co2, and the other three CN groups were free. Coordinated pyrimidine molecules bridged Co1 and Co2 (Figure 1c). The cyano-bridged Co1−W layers (Figure S3) along the *ab* plane were linked by Co2.

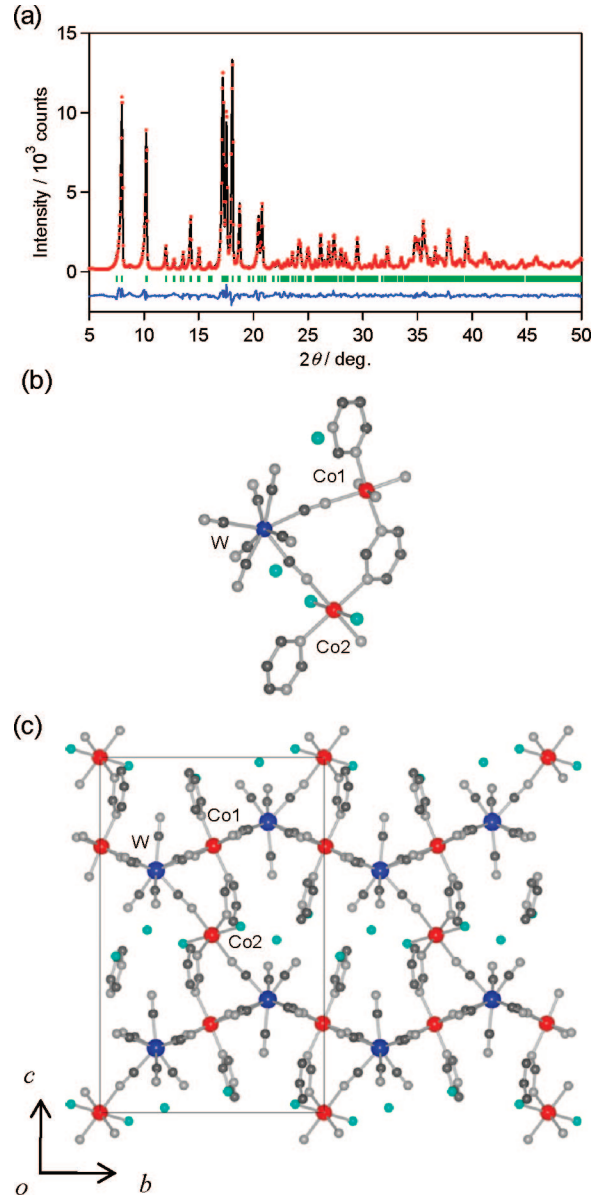

Figure 1. (a) XRD pattern of the powder form of $[\{Co^{II}(\text{pyrimidine})_2\}_2\{Co^{II}(H_2O)_2\}\{W^{V}(CN)_8\}_2]\cdot 4H_2O$ (**1**) and Rietveld analysis. Red dots, black line, and blue line are the observed plots, calculated pattern, and their difference, respectively. Green bars represent the calculated positions of the Bragg reflections. (b) Schematic illustration of the coordination environments around Co and W. (c) View perpendicular to the grid layer. Red, blue, dark gray, light gray, and light green balls represent Co, W, C, N, and O, respectively.

Compound 2. Elemental analyses showed that the formula of **2** was identical to that of **1**, but the morphology differed from **1**. SEM image showed that **2** was composed of block-type microcrystals with an average size of 3.8 × 1.5 × 1.5 μm (Figure S1b). Rietveld analysis of the XRD pattern of **2** in the powder form showed that the cell parameters of the unit cell differed slightly from those of **1**, i.e., monoclinic crystal structure in the $P2_1/n$ space group ($a = 7.1756(10)$ Å, $b = 14.650(2)$ Å, $c = 23.159(3)$ Å, $\beta = 91.099(5)°$, and $Z = 2$) with refinements of $R_{wp} = 10.14\%$ and $R_p = 7.04\%$ (Figure S4).

(26) Izumi, F.; Momma, K. *Solid. State Phenom.* **2007**, *130*, 15.

Table 1. Crystallographic Data of 1 by Rietveld Analysis of the Powder XRD Pattern

empirical formula	$C_{32}H_{28}Co_3N_{24}O_6W_2$
M	1389.23
crystal system	monoclinic
space group	$P2_1/n$
a/Å	7.5758(12)
b/Å	13.875(2)
c/Å	22.230(4)
β/deg	95.709(7)
V/Å^3	2325.1(18)
d_{calcd}/g cm^{-3}	1.943
T/K	296
Z	2
R_{wp}/R_p	0.0996/0.0694

X-ray single-crystal analysis[20c] of **2** showed that this phase belonged to the monoclinic structure of $P2_1/n$ space group (a = 7.179(1) Å, b = 14.634(2) Å, c = 23.134(7) Å, β = 91.121(14)°, and Z = 2) (Figure 2). The structure was solved by direct methods and refined on F^2 to $R1(wR2)$ = 0.0976(0.2241) using 3267 reflections with $I > 2.00\ \sigma(I)$ (Table 2). The non-hydrogen atoms were anisotropically refined. The hydrogen atoms of pyrimidine were refined isotropically. The asymmetric unit consisted of a $[W(CN)_8]^{3-}$ anion, a $[Co1(pyrimidine)(H_2O)]^{2+}$ cation, one-half of a $[Co2(H_2O)_2]^{2+}$ cation, a zeolitic water, and a noncoordinated

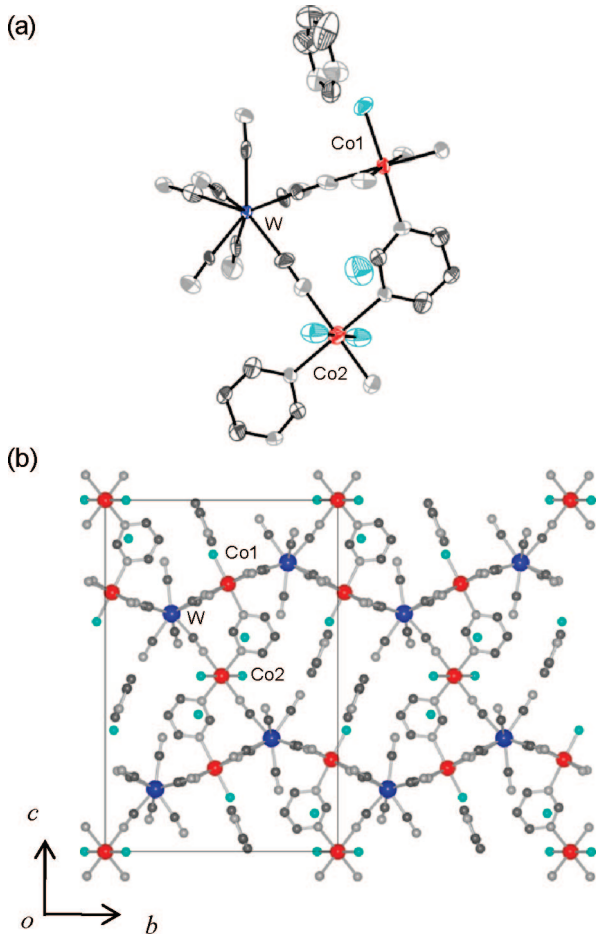

Figure 2. X-ray single crystal structure of $[\{Co^{II}(pyrimidine)(H_2O)\}_2\{Co^{II}(H_2O)_2\}\{W^{V}(CN)_8\}_2](pyrimidine)_2\cdot 2H_2O$ (**2**). (a) Thermal ellipsoid plots showing the coordination environments around Co and W. Displacement ellipsoids are drawn at a 50% probability level. (b) View perpendicular to the grid layer. Red, blue, gray, light gray, and light blue balls represent Co, W, C, N, and O, respectively. H atoms are omitted for clarity.

Table 2. Crystallographic Data of 2 by X-ray Single-Crystal Analysis

empirical formula	$C_{32}H_{28}Co_3N_{24}O_6W_2$
M	1389.23
crystal dimensions/mm^3	0.15 × 0.10 × 0.02
crystal system	monoclinic
space group	$P2_1/n$
a/Å	7.179(2)
b/Å	14.634(5)
c/Å	22.134(7)
β/deg	91.121(14)
V/Å^3	2324.9(13)
d_{calcd}/g cm^{-3}	1.984
T/K	296
Z	2
μ(Mo Kα)/cm^{-1}	6.052
reflections collected	20545
unique	3267 (R_{int} = 0.103)
$R/wR2$ (all data)	0.0976/0.2241
GOF on F^2	0.987

pyrimidine (Figure 2a). The coordination geometries of the Co (Co1 and Co2) and W sites were pseudo-octahedron (D_{4h}) and bicapped trigonal prism (C_{2v}), respectively. The four equatorial positions of Co1 were occupied by cyanide nitrogen atoms of $[W(CN)_8]$, while the apical positions were occupied by one nitrogen atom of the pyrimidine and one oxygen atom of the water ligand. Co2 was coordinated to two nitrogen atoms of $[W(CN)_8]$, two oxygen atoms of the water ligands, and two nitrogen atoms of the pyrimidines. The five CN groups of $[W(CN)_8]$ were bridged to four Co1 and one Co2, and the other three CN groups were free. The coordinated pyrimidine molecules bridged Co1 and Co2 (Figure 2b). The cyano-bridged Co1−W layers along the *ab* plane (Figure S5) were linked by Co2. The noncoordinated pyrimidine molecule was penetrated in the interstitial site. Compounds **1** and **2** have similar metal−organic frameworks but differ in the coordination around Co1, i.e., $Co1(NC)_4(pyrimidine)_2$ in **1** and $Co1(NC)_4(pyrimidine)(H_2O)$ in **2**.

3.2. Temperature Dependence of the Physical Properties. *Compound 1.* Figure 3 shows the product of the molar magnetic susceptibility (χ_M) and temperature (T) vs T plots of **1**. The $\chi_M T$ value decreased at 208 K (= $T_{1/2\downarrow}$) as the sample was cooled at a rate of −1.0 K min^{-1}. Conversely, as the sample was warmed at a rate of +1.0 K min^{-1}, the $\chi_M T$ value increased around 298 K (= $T_{1/2\uparrow}$) and returned to the initial value. The thermal hysteresis value ($\Delta T \equiv T_{1/2\downarrow} - T_{1/2\downarrow}$) was surprisingly large, 90 K. The colors of the HT phase at 300 K and the LT phase at 10 K were red and blue, respectively. Figure 4 shows the temperature dependence of $\nu_{W\text{-}CN}$ in the IR spectrum. The weak peaks at $\nu_{W\text{-}CN}$ = 2185,

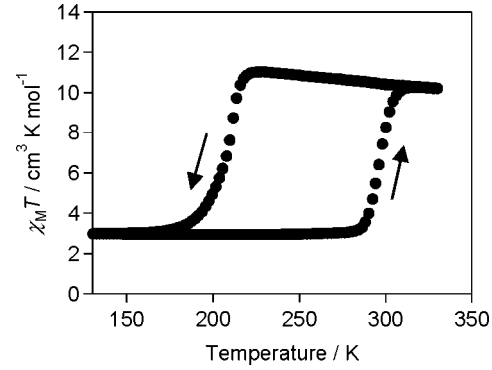

Figure 3. Thermal phase transition in **1**. $\chi_M T - T$ plots at 5000 Oe.

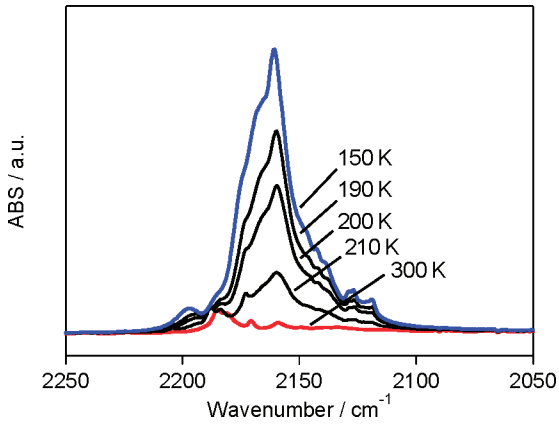

Figure 4. Temperature dependence of the CN stretching peaks in IR spectra of **1** with decreasing temperature.

2171, and 2160 cm^{-1} of the HT phase at 300 K changed into strong peaks at $\nu_{W\text{-}CN}$ = 2196, 2166, 2161, 2143, 2128, and 2119 cm^{-1} of the LT phase at 150 K. The observed $\nu_{W\text{-}CN}$ peaks of the LT phase suggest that the oxidation state of W is four (Figures S6 and S7). The results of $\chi_M T-T$ plots and temperature dependence of the IR spectra indicate that the observed temperature-induced phase transition from the HT phase to the LT phase is due to the change in the electronic state from $Co^{II}_{hs}(S = 3/2)-W^{V}(S = 1/2)$ to $Co^{III}_{ls}(S = 0)-W^{IV}(S = 0)$ where hs and ls are the high-spin and low-spin states, respectively; i.e., a charge-transfer-induced phase transition occurs. Because of stoichiometric limitations, 1/3 of the cobalt ions should remain as Co^{II}_{hs}, and thus, the LT phase is expressed as $(Co^{II}_{hs})(Co^{III}_{ls})_2$-$[W^{IV}(CN)_8]_2$(pyrimidine)$_4\cdot 6H_2O$. Figure 5 shows the UV–vis reflectance spectra of the HT and LT phases. In the HT phase, the absorption bands were observed around 500 nm. The waveform separation of the HT phases indicates that the absorption spectra can be fitted by the peaks of the LMCT (CN-W^{V}) band,[27] the MMCT ($Co^{II}_{hs} \rightarrow W^{V}$) band, and the d−d transition of Co^{II}_{hs} bands as shown in Table 3. In contrast, the absorption bands in the LT phases were observed at 770 nm. The valence state of LT phase is assigned to be $(Co^{II}_{hs})(Co^{III}_{ls})_2[W^{IV}(CN)_8]_2$(pyrimidine)$_4\cdot$ $6H_2O$ from the results of charge balance, SQUID and IR spectra, and then the absorption spectrum of LT phase contains 1/3 of Co^{II}_{hs} d−d transition compared to HT phase. The absorption spectra of the LT phase can be fitted by the bands of the d−d transition of Co^{II}_{hs} band, the d−d transition of W^{IV},[27] the d−d transition of Co^{III}_{ls}, and the MMCT ($W^{IV} \rightarrow Co^{III}_{ls}$) band.

Compound **2.** The $\chi_M T-T$ plots for **2** did not show a drop with decreasing temperature at a rate of −1.0 K min^{-1} (Figure 6a). In **2**, the charge-transfer phase transition was not observed. When **2** was cooled to a very low temperature under an external magnetic field of 10 Oe, it exhibited spontaneous magnetization with a Curie temperature (T_C) of 32 K (Figure 6b). The magnetization as a function of the external magnetic field at 2 K indicated that the saturated magnetization (M_s) value was 8.0 μ_B and the coercive field (H_c) value was 12 kOe (Figures 6c and S8). Considering that the ground Kramers doublet of an octahedral Co^{II} is

(27) Isci, H.; Mason, W. R. *Inorg. Chim. Acta* **2004**, *357*, 4065.

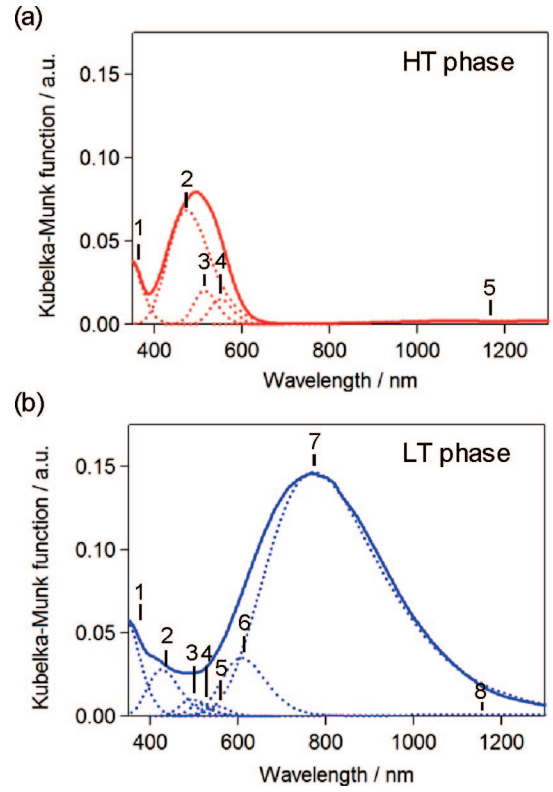

Figure 5. UV–vis reflectance spectra (solid line) and their waveform separations (dotted lines) of the HT (a) and LT (b) phases of **1**.

Table 3. Analysis of UV–Vis Reflectance Spectra of 1

	peak no.	λ/nm	peak area[a]	type of optical transition	
HT phase	1	343	0.263	W^{V} LMCT	$^2B_1 \rightarrow {}^2A_2, {}^2E$
	2	473	0.461	MMCT	$Co^{II} \rightarrow W^{V}$
	3	514	0.066	Co^{II} d−d	$^4T_{1g} \rightarrow {}^4T_{1g}$
	4	551	0.041	Co^{II} d−d	$^4T_{1g} \rightarrow {}^4A_{2g}$
	5	1170	0.016	Co^{II} d−d	$^4T_{1g} \rightarrow {}^4T_{2g}$
LT phase	1	369	0.408	W^{IV} d−d	$^1A_1 \rightarrow {}^1E$
	2	430	0.178	W^{IV} d−d	$^1A_1 \rightarrow {}^3E$
	3	496	0.040	Co^{III} d−d	$^1A_{1g} \rightarrow {}^1T_{2g}$
	4	514	0.023	Co^{II} d−d	$^4T_{1g} \rightarrow {}^4T_{1g}$
	5	551	0.016	Co^{II} d−d	$^4T_{1g} \rightarrow {}^4A_{2g}$
	6	608	0.153	Co^{III} d−d	$^1A_{1g} \rightarrow {}^1T_{1g}$
	7	772	1	MMCT	$W^{IV} \rightarrow Co^{III}$
	8	1170	0.006	Co^{II} d−d	$^4T_{1g} \rightarrow {}^4T_{2g}$

[a] Peak area is standarized by the peak area of peak no.7 of LT phase.

populated, the sublattice magnetization of Co^{II} is 2.17 μ_B ($g_{Co}J_{Co}$ = 13/3 × 1/2), and the sublattice magnetization of W^{V} is 1 μ_B assuming g_W = 2. Hence, the theoretical saturation magnetization for the ferromagnetic ordering is 8.5 μ_B for the given formula. Therefore, the observed magnetization value at 2 K suggests that the magnetic spins on Co^{II} and W^{V} ferromagnetically interact (Figure S9).

3.3. Photomagnetic Effect of 1. *Photoreversible Changes in SQUID and IR Spectra.* The photomagnetic effect of the LT phase of **1** was investigated using a SQUID magnetometer. Because the LT phase possesses an MMCT band of $Co^{III} \rightarrow W^{IV}$ at the center of λ_{max}= 772 nm (Figure 5b), a 840 nm laser was used as the light source. Figure 7 shows the field-cooled magnetization (FCM) curves before and after irradiating at 5 K in an external magnetic field of 10 Oe. The photoinduced (PI) phase exhibited a spontaneous magnetization with a T_C of 40 K. The magnetization vs

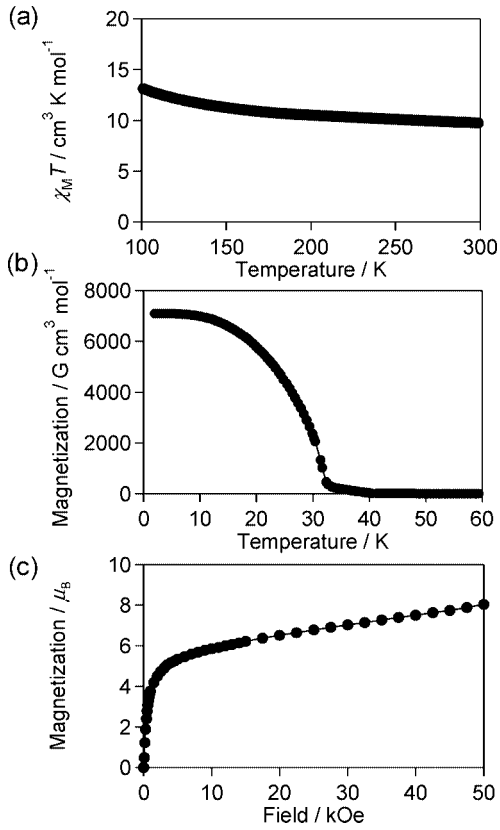

Figure 6. Magnetic properties of **2**: (a) $\chi_M T-T$ plots at 5000 Oe; (b) field-cooled magnetization curve at 10 Oe; (c) saturation magnetization curve at 2 K.

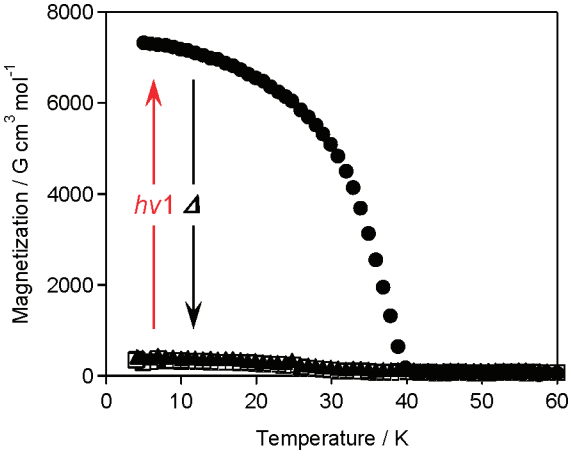

Figure 7. Photoinduced magnetization for **1**. FCM curves at 10 Oe: before irradiating (□), after irradiating with $h\nu 1$ (λ = 840 nm, 50 mW/cm^2, 160 min) (●), and after thermal treatment (▲) up to 150 K.

external magnetic field plots after irradiating showed a magnetic hysteresis loop with a H_c of 12 kOe at 2 K (Figure 8). The saturation magnetization of the PI phase was 7.2 μ_B at 5 T. Because the theoretical saturation magnetization for the ferromagnetic ordering is 8.5 μ_B for the formula, as mentioned above, the magnetic spins on Co^{II} and W^{V} are suggested to ferromagnetically interact. The photoinduced magnetization persisted for at least 1 day at 3 K after turning off the light, but the photoinduced magnetization relaxed to the initial value upon a thermal treatment up to 150 K, indicating that irradiation can increase the magnetization, but a thermal treatment can recover it. The photoreverse process

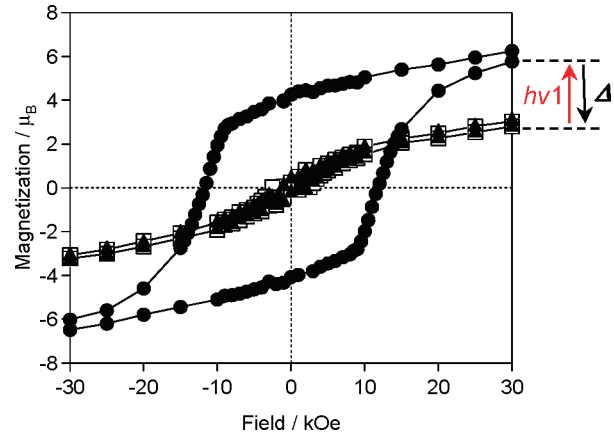

Figure 8. Magnetic hysteresis loops of **1** at 2 K: before irradiating (□), after irradiating with $h\nu 1$ (λ = 840 nm, 50 mW/cm^2, 120 min) (●), and after thermal treatment (▲) up to 150 K.

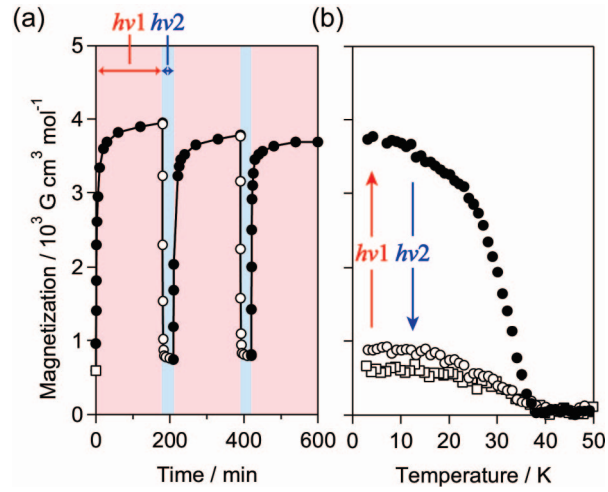

Figure 9. Photoreversible magnetization for **1**. (a) Magnetization vs irradiation time plots at 10 K by alternating with $h\nu 1$ (λ = 840 nm, 100 mW/cm^2) and $h\nu 2$ (λ = 532 nm, 50 mW/cm^2) lights. (b) Magnetization vs temperature plots before (□), after irradiating with $h\nu 1$ (●), and after irradiating with $h\nu 2$ (○).

of this photoinduced magnetization was investigated. We irradiated 532 nm laser light (50 mW cm^{-2}) to the PI phase. The magnetization values decreased as shown in Figure 9. This photoreversibility of the magnetization was repeatedly observed.

Figure 10 shows the IR spectra when alternately irradiating with 840 and 532 nm laser lights at 3 K. Irradiating the LT phase with 840 nm light caused the IR peak of Co^{III}−NC–W^{IV} at 2163 cm^{-1} to decrease. In contrast, when the PI phase was successively irradiated with 532 nm laser light, the IR peak of Co^{III}−NC–W^{IV} recovered, indicating that PI phase has a similar electronic state as the HT phase and that PI phase is converted to LT phase by the different light.

Mechanism of Photoreversible Magnetism. The observed reversible photomagnetic effect on **1** can be explained by the scheme shown in Figure 11. The forward process is caused by the optical phase transition from the LT phase to the PI phase. That is, irradiating the MMCT ($W^{IV} \rightarrow Co^{III}$) band induces a valence state change from the $Co^{III}_{ls}(S = 0)$−$W^{IV}(S = 0)$ state to the $Co^{II}_{ls}(S = 1/2)$−$W^{V}(S = 1/2)$ state through photoexcited state I, which subsequently

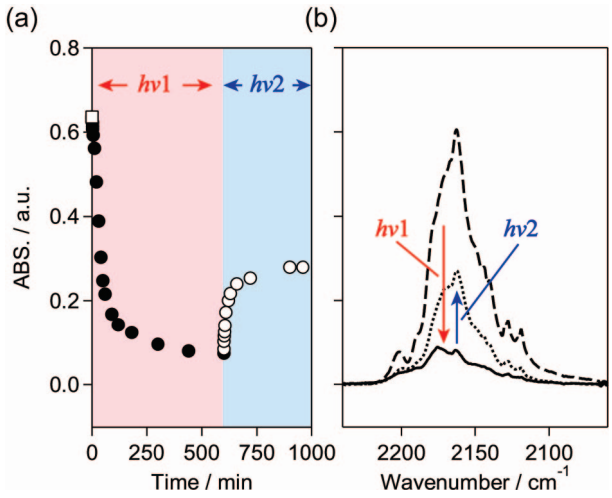

Figure 10. Photoreversible change in IR spectra of **1** at 3 K. (a) Peak intensity at 2163 cm^{-1} vs irradiation time plots upon irradiation with $h\nu1$ (λ = 840 nm, 100 mW/cm^2) (●) and $h\nu2$ (λ = 532 nm, 60 mW/cm^2) (○) lights. (b) IR spectra at 3 K before (dashed), after irradiation with $h\nu1$ (solid), and after irradiation with $h\nu2$ (dotted).

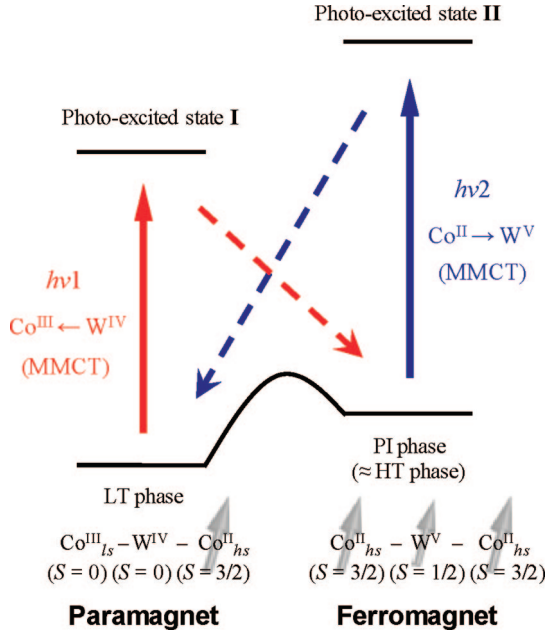

Figure 11. Schematic illustration of the mechanism of the reversible photomagnetic effect of **1**.

changes the Co^{II}_{ls} state to the Co^{II}_{hs}(S = 3/2) state and results in a spontaneous magnetization due to ferromagnetic coupling between the magnetic spins on Co^{II}_{hs}(S = 3/2) and W^{V}(S = 1/2). In contrast, the reverse process is caused by the photoinduced phase transition from the PI to the LT phase through photoexcited state II. That is, irradiating the MMCT ($Co^{II} \rightarrow W^{V}$) band induces a change from the Co^{II}_{hs}(S = 3/2)−W^{V}(S = 1/2) state to the Co^{III}_{hs}(S = 1)−W^{IV}(S = 0) state, and then the Co^{III}_{hs}(S = 1) shows a spin transition to the Co^{III}_{ls}(S = 0) state, resulting in a decreased spontaneous magnetization.

4. Conclusion

In this work, we observed $[\{Co^{II}(pyrimidine)_2\}_2\{Co^{II}(H_2O)_2\}\{W^{V}(CN)_8\}_2]\cdot 4H_2O$ exhibits a charge-transfer-induced spin transition with a large thermal hysteresis loop of 90 K and a photoreversible magnetic effect between the paramagnetic and ferromagnetic states. The PI phase shows a high T_C of 40 K and a large H_c value of 12 kOe. These values are the highest ones reported to date. This success is due to (i) the electronic structure of class II mixed-valence compounds that meet the conditions for reversible photoinduced electron transfer and (ii) the magnetic coupling of magnetic spins is strong and coordination number is large in a 3-D octacyano-bridged bimetal assemblies.

Acknowledgment. The authors thank Prof. K. Hashimoto for helpful discussions and S. Kaneko for technical support. The present research was supported in part by a Grant for the Global COE Program, "Chemistry Innovation through Cooperation of Science and Engineering", a Grant-in-Aid for Scientific Research on Priority Area "Chemistry of Coordination Space", a Grant-in-Aid for Scientific Research (B) from the Ministry of Education, Culture, Sports, Science and Technology of Japan, JSPS and RFBR under the Japan-Russia Research Cooperative Program, The Royal Society Joint Project Programme, Iketani Science and Technology Foundation, Inamori Foundation, The Kurata Memorial Hitachi Science and Technology Foundation, and The Murata Science Foundation.

Supporting Information Available: Information relating to X-ray crystallographic file in CIF format; SEM images of **1** and **2**, atomic coordinates of **1**, crystal structure and crystallographic data for $[\{Co^{II}/Cu^{II}(pyrimidine)_2\}\{Co^{II}/Cu^{II}(H_2O)_2\}\{W^{V}(CN)_8\}_2]\cdot 4H_2O$ (Co^{II}:Cu^{II} = 2:1) of a reference sample, crystal structure of **1** parallel to the grid layer, XRD pattern for the powder-form **2**, crystal structure of **2** parallel to the grid layer, the stick diagram of CN stretching frequencies of $[W^{IV}(CN)_8]^{4-}$ and $[W^{V}(CN)_8]^{3-}$, magnetic properties of **2**. This material is available free of charge via the Internet at http://pubs.acs.org.

CM703258N